Robust Classification and Analysis of Anatomical Surfaces Using 3D Skeletons

Reniers, D.; Jalba, A.; Telea, A.

Published in:
EPRINTS-BOOK-TITLE

Publication date:
2008

Eurographics Workshop on Visual Computing for Biomedicine (2008)
Charl Botha and Gordon Kindlmann and Wiro Niessen and Bernhard Preim (Editors)

Robust Classification and Analysis of Anatomical Surfaces Using 3D Skeletons

D. Reniers[1] and A. Jalba[1] and A. Telea[2]

[1]Department of Mathematics and Computer Science, Eindhoven University of Technology, the Netherlands
[2]Institute for Mathematics and Computer Science, University of Groningen, the Netherlands

Abstract

We present a method for computing a surface classifier that can be used to detect convex ridges on voxel surfaces extracted from 3D scans. In contrast to classical approaches based on (discrete) curvature computations, which can be sensitive to various types of noise, we propose here a new method that detects convex ridges on such surfaces, based on the computation of the surface's 3D skeleton. We use a suitable robust, noise-resistant skeletonization algorithm to extract the full 3D skeleton of the given surface, and subsequently compute a surface classifier that separates convex ridges from quasi-flat regions, using the feature points of the simplified skeleton. We demonstrate our method on voxel surfaces extracted from actual anatomical scans, with a focus on cortical surfaces, and compare our results with curvature-based classifiers. As a second application of the 3D skeleton, we show how a partitioning of the brain skeleton can be used in a preprocessing step for the brain surface analysis.

1. Introduction

Detecting features such as ridges and valleys in datasets such as 2D grayscale images and 3D CT and MRI volumetric scans, is an important and active area of research. Features such as edges and corners must be classified in a robust way in order to enable further analyses on such datasets, like edge-preserving denoising or robust partitioning of areas bounded by such edges. The so-called local classification of surfaces, in particular the separation of highly curved ridges from low curvature areas, is also an important prerequisite in numerous surface processing applications such as surface matching and feature-preserving simplification.

Traditionally, most surface classifiers used in practice employ one or another variation of ridge detection based on higher-order surface derivatives, such as gradients, curvature, or moments. Although a wealth of such methods exist, curvature estimations on noisy voxel surfaces is an inherently delicate process. Many such methods trade off the precision of ridge detection for stability, by using different types of filtering over (small) neighborhoods.

Curvature is intimately connected to another well-known surface descriptions: skeletons or medial axes. However, this relation has not often been used for surface classification or ridge detection, partly due to the infamously unstable nature of 3D skeletons, the difficulty of computing them in 3D, and the lack of an appropriate scale notion.

In this paper, we show that 3D skeletons can be used for robust voxel surface classification. We extend a stable 3D skeletonization method that comes with a built-in multiscale criterion so that we compute a surface classifier which separates convex ridges from smooth regions. Our method employs only integral quantities, such as Euclidean and geodesic distances, and hence is inherently robust as compared to several curvature estimators, even on noisy, low-resolution datasets. We implement the proposed method to work directly on, and uniquely with, voxel representations of the surface, skeleton, and classifier. We illustrate our method on the classification of anatomical surfaces, with a focus on cortical surfaces, and compare it with a curvature-based classifier. Finally, we show the feasibility of a robust partitioning of a 3D brain skeleton, to emphasize the high potential of 3D skeletons in further surface analysis applications.

This paper is structured as follows. Section 2 overviews related work in the area of surface classification, with a focus on brain cortex analysis. Section 3 overviews 3D skeletonization, with an emphasis on the robust multiscale method we shall extend here. Section 4 presents our new skeleton-based surface classification used for ridge detec-

tion. Section 5 shows the results of our method applied to a voxel-based brain surface, and compares it with a typical curvature-based classifier. Section 6 illustrates another potential application of 3D skeletons, by showing the robust partitioning of a 3D brain skeleton. Section 7 discusses our method and compares it with curvature-based classifiers. Section 8 concludes the paper.

2. Related work

The canonical quantity for edge detection on surfaces is the curvature tensor. Different methods exist for its evaluation on discrete surfaces, such as shown by Moreton and Séquin [MS92], Clarenz *et al.* [CDR00], and Desbrun *et al.* [DMSB00]. Besides curvature, surface classifiers can be based on related integral quantities, such as moments [CRT04]. Globally speaking, all such methods use a local surface classification, and thereby trade edge detection accuracy for stability via some built-in smoothing.

Extracting cortical surface features, such as sulci and gyri, from MR brain volumes is focus of extensive work. Such features are used in studies of inter-subject gyral and sulcal variability [GPC*99] or to identify structural and functional patterns in Alzheimer patients [THS*04].

Many methods for sulci extraction use the surface's (mean) curvature. Sulcal fundi are defined as crest lines of extremal curvature. Similar approaches can be used for gyral structures. Such methods are semi-automatic, requiring the user to define two or more points on a sulcus, which are then connected by optimizing a curvature-based cost. Several such approaches exist, using weighted geodesics [BS01], dynamic programming [KMG98], fast marching [MST04] and 3D curve-tracking [RDR00]. Evaluating curvature extrema involves higher-order derivatives, so these methods can be quite unstable on highly convoluted cortical surfaces coming as limited resolution voxel scans (see also Sec. 5). Cachia *et al.* [CMR*03] alleviate such problems using a scale-space of the underlying curvature signal, thereby trading precision for stability.

To overcome stability problems, other methods find sulcal fundi by locally maximizing the distance from the cortical surface to a bounding hull around it. The methods of [GPC*99, Loh98] find fundi as the deepest boundaries of surfaces obtained by subtracting the white and gray matter from the bounding hull. Combining curvature and distance-based criteria leads to more stable, but significantly more complex to implement, methods [KHS*07, KHS*06, TPD02, THR*01].

Although uncommon, using skeletons to detect features is not new. Hisada *et al.* [HBK01] use the skeleton in combination with denoising and filter techniques to detect salient shape features of polygonal shapes.

3. 3D Skeletonization

This section gives a brief overview of the 3D skeletonization method and associated importance measure that underlie our surface classifier which we discuss in Section 4.

3.1. Preliminaries

Let Ω be a 3D shape with closed boundary $\partial\Omega$. Let $D : \Omega \rightarrow \mathbb{R}_+$ be the distance transform, assigning to each point inside the shape the minimum distance to the boundary. Let $F : \Omega \rightarrow \mathcal{P}(\partial\Omega)$, where $\mathcal{P}$ is the power set, be the so-called feature transform, assigning to each point inside the shape the set of boundary points at minimum distance, called the *feature points*:

$$F(p \in \Omega) = \left\{ q \in \partial\Omega \;\middle|\; \|p - q\| = D(p) \right\} \tag{1}$$

The *skeleton* $\mathcal{S}$ of Ω can be defined as the locus of centers of maximally inscribed balls. At each point p on the skeleton, a maximally inscribed ball can be placed that touches the boundary in at least two points, the feature points $F(p)$:

$$\mathcal{S}(\Omega) = \left\{ p \in \Omega \;\middle|\; |F(p)| \geq 2 \right\} \tag{2}$$

This definition can be used both in 2D and 3D. In 3D, $\mathcal{S}$ is sometimes called the medial surface, or surface skeleton, to distinguish it from the curve skeleton, or centerline. In this paper, we shall compute and use the medial surface

The skeleton of a 3D shape consists of manifolds, called *sheets*, which intersect in curves, called *Y-curves* [Dam06]. Whereas sheet points have two feature points, Y-curve points have three or more feature points which are the union of the feature-point pairs of the intersecting sheets. In addition, a surface skeleton can also contain isolated curves in some degenerate cases, such as a cylinder. However, brain surfaces do not contain such structures, as they do not have a tubular structure, *i.e.* their never have circular cross-sections.

3.2. Simplified Robust Skeletons

Following from Eq. 2, skeletons are inherently sensitive to small boundary perturbations. This situation is considerably worsened in practice by sampling noise emerging from the limited resolution of 3D acquisition devices, like MRI or CT scans. 3D skeletons directly computed following Eq. 2 will exhibit a myriad of spurious sheets corresponding to small-scale boundary noise (*e.g.* tiny bumps). This is one of the main problems which has precluded their use in practical applications.

To produce robust skeletons, some skeletonization methods define an *importance* measure $\rho : \mathcal{S} \rightarrow \mathbb{R}_+$ indicating the importance of each skeletal point in representing the shape. Combined with a suitable pruning strategy, this delivers a simplified skeleton [SB98].

One successful importance measure ρ is defined as the

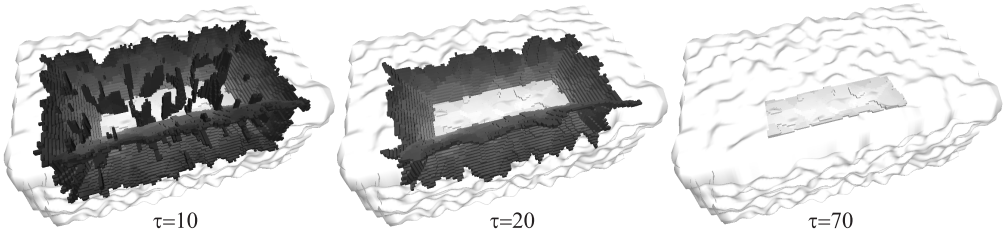

Figure 1: *Simplified skeletons $\mathcal{S}_{\tau=10}, \mathcal{S}_{\tau=20}, \mathcal{S}_{\tau=70}$ of a noisy box. The intensity encodes the importance measure ρ. Whereas $\mathcal{S}_{\tau=10}$ contains some spurious sheets, $\mathcal{S}_{\tau=20}$ is robust. In $\mathcal{S}_{\tau=70}$, only the center sheet is retained, which can be seen as a coarse-scale representation of the box.*

length of the shortest path on the surface $\partial\Omega$ between the two feature points $F(p)$ for each point $p \in \mathcal{S}$ [PH02]. This measure smoothly evolves over skeletal sheets, may contain jumps at Y-curves (cf. Fig. 1), is low on the periphery of the skeleton, and has a local maximum ridge in the middle of the skeleton [DS06]. Besides yielding robust skeletons, it can be used to obtain progressively simplified, or multiscale, skeletons by simply increasing the threshold on ρ [RVT08].

To implement such a measure for voxelized objects, we proceed as follows. The feature transform is computed using [Mul92]. Let $\overline{F}$ be the *extended* feature transform, defined as $\overline{F} = \bigcup_{x,y,z\in\{0,1\}} F(p_x + x, p_y + y, p_z + z)$. Then, the importance measure $\rho : \Omega \to \mathbb{R}_+$ is defined on the object voxels as the maximum shortest-path length between the points in the feature set $\overline{F}(p)$:

$$\rho(p) = \max_{a,b\in\overline{F}(p)} \|\gamma(a,b)\|, \tag{3}$$

where γ is the shortest path between a, b and $\|\cdot\|$ the shortest-path length, computed using an accurate length estimator [KS93] which assigns different weights to the three different voxel-neighbor types. Using ρ, the definition of the discrete simplified-skeleton $\mathcal{S}_\tau$ becomes (cf. Eq. 2):

$$\mathcal{S}_\tau(\Omega) = \{p \in \Omega \mid \rho(p) \geq \tau\}, \tag{4}$$

Empirical studies indicate that τ should set to at least 5 voxel-length units to prune the skeleton $\mathcal{S}_\tau$ of any noise due to discretization artifacts [PH02, RVT08]. The threshold τ functions as a continuous scale-parameter controlling the simplification level. Small τ values eliminate less important skeleton parts that are due to small-scale surface features or acquisition noise. Larger τ values can be used to retain the most salient parts of the skeleton. For illustration, Figure 1 shows the effect of increasing τ for a noisy 3D box.

It is important that the simplified skeletons remain connected, as skeletons should be homotopic to the original shape [Lie03]. Fortunately, the simplified skeletons are connected for the smaller values of τ, because the measure ρ is monotonic on $\mathcal{S}_\tau$ except on the local maximum ridge [DS06]. Note that the restriction of the skeletonization method to genus 0 shapes as mentioned in [RVT08] does not apply here as we do not need to compute the curve-skeleton.

4. Skeleton-based Surface Classifier

The key idea of our approach is simple: By increasing the simplification level τ, we prune the boundary of the skeleton first. Because the skeleton reaches into the *ridges* of the surface, we remove the skeleton parts whose feature points lie on and near these ridges. In this fashion, we can detect ridges by the absence of feature points.

This idea reflects an intimate connection of skeletons with curvature extrema on the surface. Specifically, the boundary points of the skeleton, *i.e.* branch tips in 2D and medial sheet edges in 3D, correspond one-to-one with curvature maxima (convex ridges) on the surface, via the feature transform. Hence, by using the skeleton and associated feature points, suitably pruned to remove noise effects, we can robustly detect such ridges, without *any* discrete curvature computation.

Let V be the set of feature points corresponding to a simplified skeleton. We call this set the *feature collection* of $\mathcal{S}_\tau$:

$$V(\mathcal{S}_\tau) = \bigcup_{p\in\mathcal{S}_\tau} \overline{F}(p), \tag{5}$$

By increasing the threshold τ on the importance measure ρ, gaps will appear in the feature collection V on and near shape convex ridges. We can detect such gaps and use them to detect the ridges. However, one complication is that the parameter τ is also used to prune spurious skeleton parts that are due to boundary noise or discretization artifacts. Here, we assume that the scale of the noise is uniform for the whole shape. Setting τ to the noise level τ_n opens V on the ridges, but also on noisy parts, which we do not want to detect as ridges. Therefore, we have to increase τ further to $\tau_n + \tau_e$: the feature collection V is opened further on ridges, but not on boundary noise. This is illustrated in Fig. 2 in the 2D case, for the sake of clarity. In Fig. 2a, the non-simplified skeleton $\mathcal{S}_0$ of a box with a small-scale noise bump is shown. The feature collection (thick lines) covers the whole boundary.

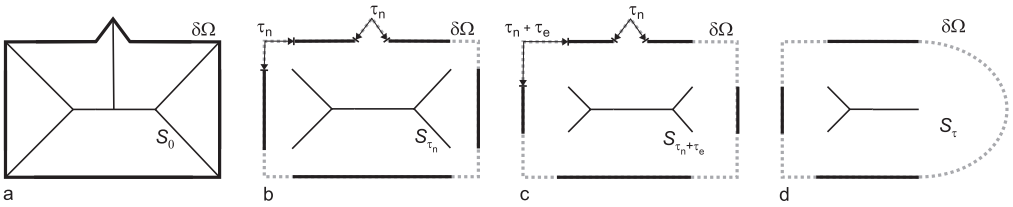

Figure 2: *Non-simplified skeleton (a). Simplified skeleton at scale τ_n (b). Simplified skeleton at scale $\tau_n + \tau_e$ (c). Large gap due to round part (d). Thick lines are feature collections V.*

When τ is set to the noise level τ_n (Fig. 2b), the openings in V on the bump and near the non-noisy convex corners have the same size, so that we cannot differentiate between the two situations. By further increasing τ to $\tau_n + \tau_e$ (Fig. 2c), V is further opened on the corners, but not on the bump.

Thus, our surface classifier is defined for each boundary point $q \in \partial\Omega$ as the geodesic distance to $V(\mathcal{S}_{\tau_n+\tau_e})$, again computed using [KS93]. Points at a distance of at least $\frac{1}{2}\tau_n$ from a feature point in V are considered ridge points. The term τ_e controls the minimum detected ridge width and should be chosen as small as possible, but at the same time large enough to account for the small inaccuracies in the feature points caused by the discretization. We verified that a conservative setting $\tau_e \geq 4$ gives good results on a wide range of objects, including 3D brain surfaces but also several other 3D synthetic and organic shapes.

The ridge-width parameter τ_e controls the minimum width of the detected ridges, but not the maximum. In case of round (blunt) parts of the shape, *e.g.* as shown in Fig. 2d, the openings in V and thus the ridges might become thicker than τ_e. The importance measure ρ varies quickly for the skeleton representing the round part, so that in the discrete case, V may opened at the round part by a slight increase of τ. This is as expected, since it is not possible to specify an exact location of an edge over blunt parts having no curvature variation.

5. Results

In this section, we illustrate our surface classification method on a brain cortex surface, computed from a MRI scan of 256^3 voxels resolution. Figure 3 shows the curvature-based classifier proposed by Taubin [Tau95] on a triangle mesh of the brain surface. To reduce small-scale noise artifacts we apply the diffusion (heat) equation geodesically to the cortical surface. To take into account the fact that the underlying grid is irregular, we use the approach in [DMSB99], equivalent to anisotropic diffusion on regular grids. The three different images in Fig. 3 correspond to increasingly longer diffusion times t, which are equivalent to increasingly larger Gaussian filters [CRT04].

Figure 6 shows our skeleton-based surface classifier, computed on three progressively simplified skeletons, as described in Sec. 4. The corresponding skeletons, and their simplification levels τ, are shown separately in Fig. 7. The simplification levels τ are chosen so that they match the sizes of the Gaussian filters that describe the curvature smoothing in Fig. 3. We notice several things. First, the simplification level τ for the skeleton-based classifier has a very similar effect to the Gaussian filtering, or smoothing time t, for the curvature classifier: Small values yield sharper (but potentially noisier) ridges, larger values yield smoother, but thicker, ridges. However, we also see that the skeleton-based detector separates the convex gyral ridges (curvature maxima) from the quasi-flat and concave regions quite sharply, even at low simplification levels, whereas the curvature-based classifier produces results where the separation is less clear. The skeleton-based classifier is also able to produce noise-free results directly in voxel space (Fig. 6 top), whereas the curvature classifier used here (and other similar ones) need to construct a local polygonal, or local tangent-plane, approximation of the voxel data.

Figure 4 illustrates our 3D skeleton and surface classifier on a hip dataset, to demonstrate the applicability of our method for different datasets besides cortical surfaces, including shapes with tunnels. Just as for the brain dataset, we see the clear separation of convex ridges (edges) from smooth regions.

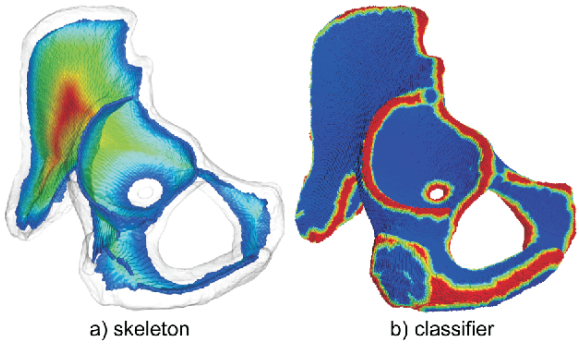

Figure 4: *Surface classification of the hip dataset*

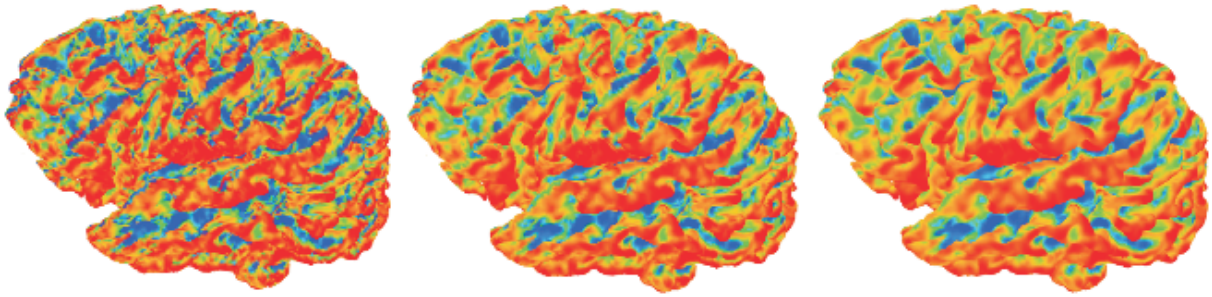

Figure 3: *Brain surface classification using a smoothed curvature estimator (blue=low curvature, red=high curvature)*

6. Brain Skeleton Partitioning

Besides computing a robust surface classifier, the 3D skeleton can be used as a preprocessing step in other applications, such as robust brain surface partitioning. The key principle enabling this is as follows. Consider the set of medial sheets that form a 3D skeleton. The intersections of two (or more) such medial sheets is called a medial intersection curve or *Y-curve*. The set of all Y-curves for a given 3D skeleton creates a graph-like structure, called the *Y-network* [Dam06]. Y-curves from this network map to important geometric events on the original surface. Specifically, curves which have one endpoint not connected to another Y-curve are the intersection of two (or more) medial sheets which correspond to bumps (convex ridges) on the original surface, *i.e.* gyri in the case of a brain. Curves whose both endpoints are connected to other Y-curves correspond to the intersection of at least two medial sheets of which at least one is 'internal', *i.e.* does not map to a convex ridge.

Hence, if we were able to partition the 3D skeleton in distinct sheets, and also extract the Y-network, we could use this information to further partition the brain geometrical structure, as outlined above. To perform this partitioning, several methods could be used. Topology-based criteria using local (3-by-3 or 5-by-5) templates can be employed to detect the medial intersection curves based on the discrete connectivity patterns of the skeleton voxels, as described *e.g.* in [MBA93,GK04], among others. However, template-based methods can have robustness problems *e.g.* in the case of multiple-sheet intersections.

To robustly partition the brain skeleton, we use a different distance-based approach, described in [RT08]. In brief, this method works as follows. First, we compute a simplified feature-transform which groups, for each skeleton voxel, feature voxels located on the surface at a geodesic distance closer than the skeleton simplification threshold τ. Second, we detect Y-curve voxels as those skeleton voxels whose simplified feature-transform has at least three groups of disconnected feature voxels. This is actually nothing else than a robust voxel-based implementation of the continuous criterion saying that an Y-curve point corresponds to at least three distinct feature points on the surface. Using the robust Y-curves we partition the simplified skeleton into distinct medial sheets.

Figure 5 shows the results of the 3D skeleton partitioning for the same brain dataset as used before. The top row shows the different medial sheets, each colored with a different color from its neighbor sheets, to distinguish them. The resulting sheets are cleanly (and clearly) separated from each other. The bottom row shows the Y-network for the same skeleton partitioning, where each Y-curve has a different color from its neighbors. Similar to the sheets, the Y-curves are clearly separated from each other.

Although we do not show it in this paper, the high quality of the 3D skeleton partitioning results makes them readily usable for further brain surface analyses. For example, one could detect the borders of each 3D sheet in Fig. 5 top, project these on the brain surface using the feature transform which we already computed (Sec. 3.1), and thereby obtain the ridge-curves of the gyral structures. Secondly, the endpoints of the Y-curves in Fig. 5 top which belong to a single curve (the 'loose' ends of those curves) correspond, via the feature transform, to brain surface points where three gyral structures meet, as explained above.

7. Discussion

As already mentioned in Sec. 4, there is a strong connection between skeletons and convex shape features. Hence, our skeleton-based surface classifier shares several properties with curvature-based classifiers: sharp ridges (edges) are detected more precisely than soft, blunt ridges; there is an analogy between Gaussian filtering of the curvature signal and geodesic-distance-based simplification of the skeleton, whereby the Gaussian filter size and the skeleton importance threshold both act as scale parameters.

However, there are also important differences. Our skeleton-based classifier uses only integral computations, and is hence inherently more robust than derivative-based curvature methods. Also, the skeleton classifier can be seen as a *quasi-global* operator, since our importance-based

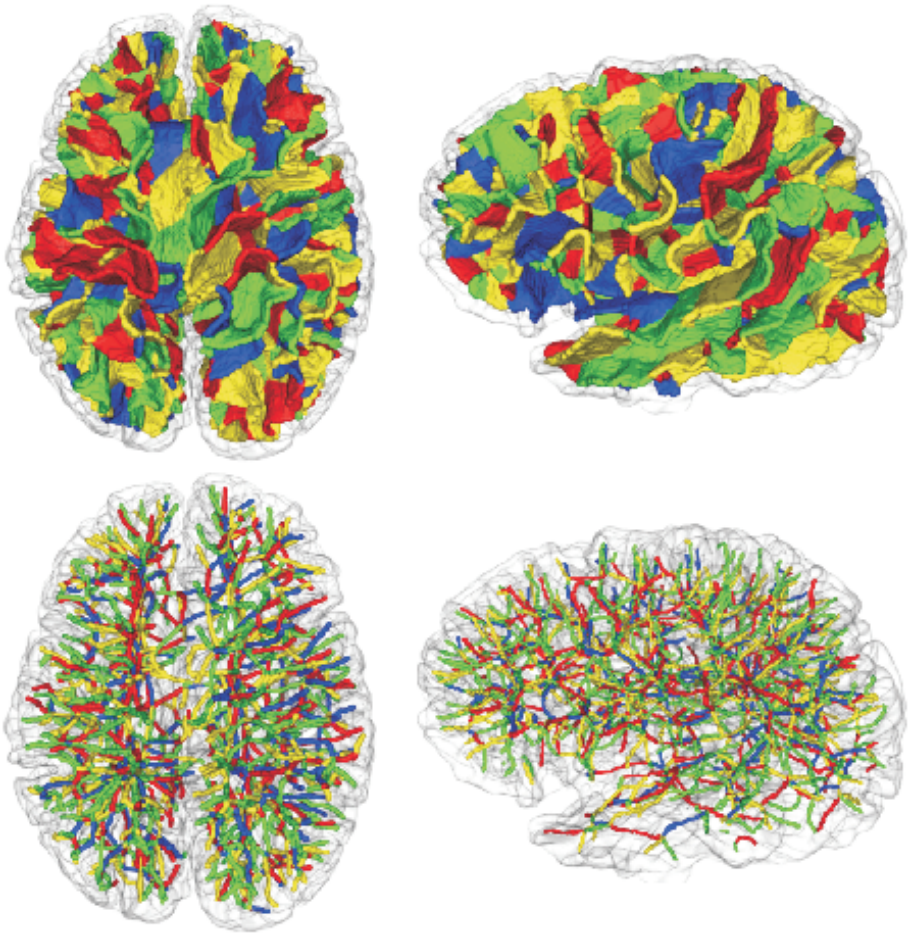

Figure 5: *Brain skeleton partitioning. Top: partitioned medial sheets (color-coded). Bottom: medial intersection curves (color-coded)*

metric 'gathers' surface information that may come from the same, but also very different, zones of the surface (see [RVT08]). In contrast, curvature estimators are strongly local, as they only analyze a small neighborhood at each surface point. Together, these facts explain the difference in robustness of the considered classifiers.

So far, we have shown how we can use skeletons to detect curvature *maxima*, or convex ridges. Detection of minima, or concave ridges, such as the sulcal fundi of a cortex surface, is equally simple: For this, we only have to use the skeleton of the volume's background, all other details of the method staying the same. Computing the background skeleton is equally easy and stable.

Concerning the computational efficiency: A brute-force, not optimized, implementation of the 3D skeletonization algorithm [RVT08] takes around 12 minutes on the 256^3 dataset, on a Windows PC at 3.0 GHz. An optimized implementation should be several times faster. After the skeleton is available, the computation of the surface classifier is fast (10-15 seconds).

8. Conclusions

In this paper we argued that 3D skeletons, which are often seen as unreliable and unstable, can be used to perform a number of basic processing operations on medical datasets. As an example of such an operation, we showed that robust, multi-scale skeletonization of the cortical surface provides a robust and effective means for the classification of voxel-based surfaces into highly convex (ridge) regions and smooth areas. We show that skeleton-based classifiers are less sensitive to discretization noise, due to their integral-based construction, as compared to curvature-based classifiers which use derivatives. We illustrate our method on different voxel datasets obtained from medical imaging scans. We also discuss how our classifier, and the underlying skeleton, can be used as a first step in brain cortex analysis.

Future work involves the actual utilization of our classifier for concrete medical imaging applications, such as the extraction of sulcal fundi curves and surface segmentation, as well as a more rigorous mathematical analysis of the connection between our classifier and curvature metrics.

References

[BS01] BARTESAGHI A., SAPIRO G.: A system for the generation of curves on 3d brain images. *Human Brain Mapping 14*, 1 (2001), 1–15.

[CDR00] CLARENZ U., DIEWALD U., RUMPF M.: Anisotropic diffusion in surface processing. In *Proc. IEEE Visualization* (2000), pp. 397–405.

[CMR*03] CACHIA A., MANGIN J.-F., RIVIÈRE D., KHERIF F., BODDAERT N., ANDRADE A., PAPADOPOULOS-ORFANOS D., POLINE J.-B., BLOCH I., ZILBOVICIUS M., SONIGO P., BRUNELLE F., RÃL'GIS J.: A primal sketch of the cortex mean curvature: a morphogenesis based approach to study the variability of the folding patterns. *IEEE Trans. Med. Imag. 22*, 6 (2003), 754–765.

[CRT04] CLARENZ U., RUMPF M., TELEA A.: Robust feature detection and local classification of surfaces based on moment analysis. *IEEE TVCG 10*, 5 (2004), 516–524.

[Dam06] DAMON J.: Global medial structure of regions in R^3. *Geometry and Topology 10* (2006), 2385–2429.

[DMSB99] DESBRUN M., MEYER M., SCHRÖDER P., BARR A. H.: Implicit fairing of irregular meshes using diffusion and curvature flow. In *Proc. ACM SIGGRAPH* (1999), ACM Press/Addison-Wesley Publishing Co., pp. 317–324.

[DMSB00] DESBRUN M., MEYER M., SCHROEDER P., BARR A.: Anisotropic feature-preserving denoising of height fields and bivariate data. In *Proc. Graphics Interface* (2000).

[DS06] DEY T. K., SUN J.: Defining and computing curve-skeletons with medial geodesic function. In *Proc. of Eurographics Symposium on Geometry Processing* (2006), pp. 143–152.

[GK04] GIBLIN P., KIMIA B.: A formal classification of 3d medial axis points and their local geometry. *IEEE TPAMI 26*, 2 (2004), 238–251.

[GPC*99] GOUALHER G., PROCYK E., COLLINS D., VENUGOPAL R., BARILLOT C., EVANS A.: Automated extraction and variability analysis of sulcal neuroanatomy. *IEEE Trans. Med. Imag. 18*, 3 (1999), 206–217.

[HBK01] HISADA M., BELYAEV A. G., KUNII T. L.: A skeleton-based approach for detection of perceptually salient features on polygonal surfaces. *Computer Graphics Forum 21*, 4 (2001), 689–700.

[KHS*06] KAO C.-Y., HOFER M., SAPIRO G., STERN J., ROTTENBERG D. A.: A geometric method for automatic extraction of sulcal fundi. In *Proc. ISBI'06* (2006), IEEE (electronic), pp. 1168–1171.

[KHS*07] KAO C. Y., HOFER M., SAPIRO G., STERN J., REHM K., ROTTENBERG D. A.: A geometric method for automatic extraction of sulcal fundi. *IEEE Trans. Med. Imag. 26*, 4 (2007), 530–540.

[KMG98] KHANEJA N., MILLER M., GRENANDER U.: Dynamic programming generation of curves on brain surfaces. *IEEE TPAMI 20*, 11 (1998), 1260–1265.

[KS93] KIRYATI N., SZÉKELY G.: Estimating shortest paths and minimal distances on digitized three-dimensional surfaces. *Pattern Recognition 26* (1993), 1623–1637.

[Lie03] LIEUTIER A.: Any open bounded subset of $\mathbb{R}^3$ has the same homotopy type as its medial axis. In *Proc. ACM SPM* (2003), pp. 65–75.

[Loh98] LOHMANN G.: Extracting line representations of sulcal and gyral patterns in MR images of the human brain. *IEEE Trans. Med. Imag. 17*, 6 (1998), 1040–1048.

[MBA93] MALANDAIN G., BERTRAND G., AYACHE N.: Topological segmentation of discrete surfaces. *IJCV 10*, 2 (1993), 183 – 197.

[MS92] MORETON H., SÉQUIN C.: Functional optimization for fair surface design. In *Proc. ACM SIGGRAPH* (1992), pp. 167–176.

[MST04] MÉMOLI F., SAPIRO G., THOMPSON P.: Implicit brain imaging. *Neuroimage 23*, 1 (2004), 179–188.

[Mul92] MULLIKIN J. C.: The vector distance transform in two and three dimensions. *CVGIP: Graphical Models and Image Processing 54*, 6 (1992), 526–535.

[PH02] PROHASKA S., HEGE H.-C.: Fast visualization of plane-like structures in voxel data. In *Proc. IEEE Visualization* (2002), pp. 29–36.

[RDR00] RENAULT C., DESVIGNES M., REVENU M.: 3d curves tracking and its application to cortical sulci detection. In *ICIP* (2000), pp. 491–494.

[RT08] RENIERS D., TELEA A. C.: Segmenting simplified surface skeletons. In *Proc. DGCI* (2008), Springer, pp. 262–274.

[RVT08] RENIERS D., VAN WIJK J., TELEA A.: Computing multiscale curve and surface skeletons of genus 0 shapes using a global importance measure. *IEEE TVCG 14*, 2 (2008), 355–368.

[SB98] SHAKED D., BRUCKSTEIN A. M.: Pruning medial axes. *Computer Vision and Image Understanding 69*, 2 (1998), 156–169.

[Tau95] TAUBIN G.: Estimating the tensor of curvature of a surface from a polyhedral approximation. In *ICCV '95: Proceedings of the Fifth International Conference on Computer Vision* (1995), IEEE Computer Society, pp. 902–9907.

[THR*01] TAO X., HAN X., RETTMANN M. E., PRINCE J. L., DAVATZIKOS C.: Statistical study on cortical sulci of human brains. In *IPMI '01: Proceedings of the 17th International Conference on Information Processing in Medical Imaging* (London, UK, 2001), Springer-Verlag, pp. 475–487.

[THS*04] THOMPSON P. M., HAYASHI K. M., SOWELL E. R., GOGTAY N., GIEDD J. N., RAPOPORT J. L., DE ZUBICARAY G. I., JANKE A. L., ROSE S. E., SEMPLE J., DODDRELL D. M., WANG Y., VAN ERP T. G., CANNON T. D., TOGA A. W.: Mapping cortical change in alzheimer's disease, brain development, and schizophrenia. *Neuroimage 23 Suppl 1* (2004), 2–18.

[TPD02] TAO X., PRINCE J., DAVATZIKOS C.: Using a statistical shape model to extract sulcal curves on the outer cortex of the human brain. *IEEE Trans. Med. Imag. 21*, 5 (2002), 513–524.

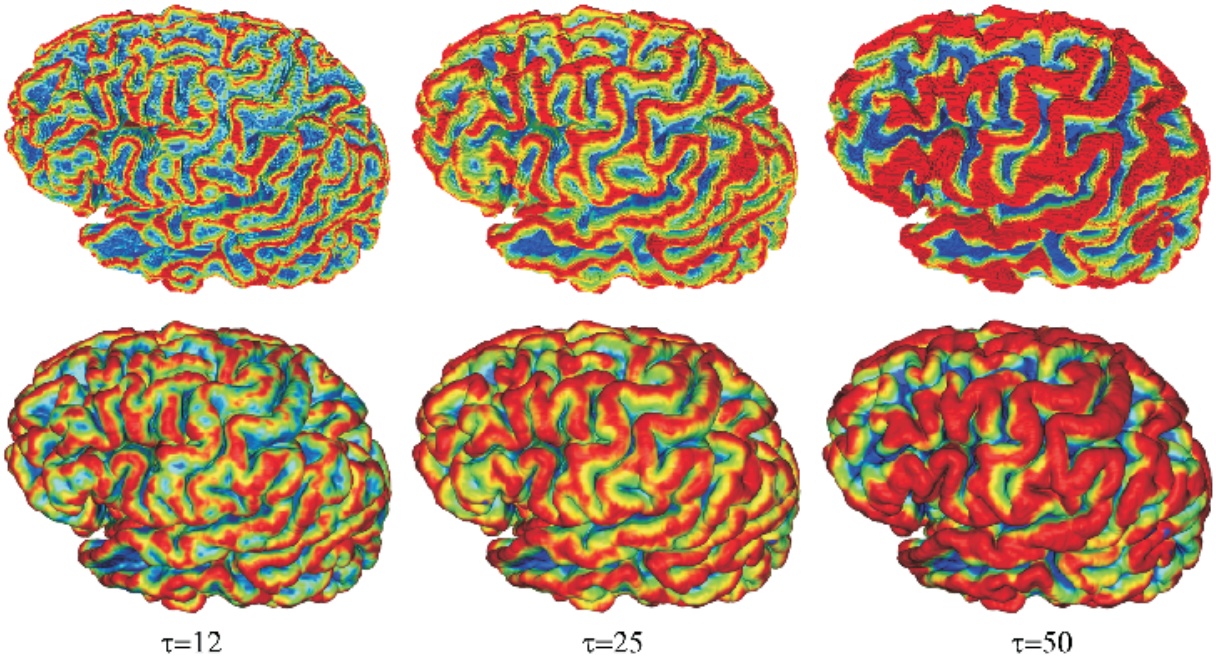

Figure 6: *Brain surface classification, different skeleton simplification levels* τ *(see Sec. 5). Top: actual voxel classifier computed. Bottom: ray-traced images of the same classifier*

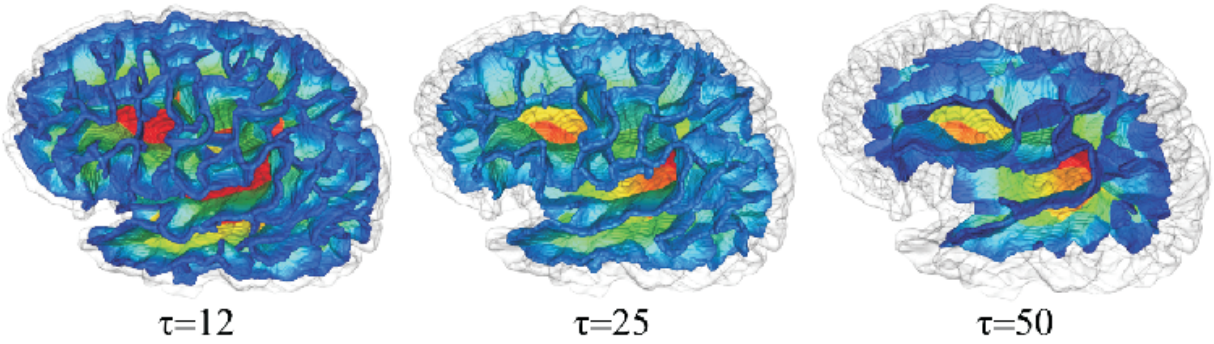

Figure 7: *Brain surface skeleton at three different simplification levels, colored by skeleton importance* ρ